THE JOURNAL OF PHYSICAL CHEMISTRY C
A JOURNAL OF THE AMERICAN CHEMICAL SOCIETY

pubs.acs.org/JPCC Article

Electrochemically Mediated Au−C(sp^2) Anchors for Molecular Electronics

Rajarshi Samajdar,○ Hao Yang,○ Seungjoo Yi,○ Chun-I. Wang,⊗ Seth T. Putnam,⊗ Michael A. Pence, Gavin S. Lindsay, Moeen Meigooni, Xiaolin Liu, Jitong Ren, Jeffrey S. Moore, Emad Tajkhorshid, Andrew A. Gewirth, Joaquín Rodríguez-López, Nicholas E. Jackson, and Charles M. Schroeder*

Cite This: *J. Phys. Chem. C* 2025, 129, 17458−17471 Read Online

ACCESS | Metrics & More | Article Recommendations | Supporting Information

ABSTRACT: Terminal anchor groups play a key role in the stability and electronic properties of molecular junctions. Single molecule junctions typically consist of two preinstalled terminal anchors linking organic molecules to metal electrodes. Here, we show that *p*-terphenyl derivatives containing only a single terminal anchor show conductance features similar to junctions with two preinstalled terminal anchors. A set of *p*-terphenyl derivatives with one terminal anchor was prepared using automated chemical synthesis and characterized using single molecule electronics experiments, molecular dynamics (MD) simulations, bulk electrochemistry and spectroscopy, and nonequilibrium Green's function-density functional theory (NEGF-DFT) calculations. Our results show that 4-amino-*p*-terphenyl (PPP) and related analogs exhibit a well-defined high conductance state that is diminished or absent in other *p*-terphenyl derivatives lacking a preinstalled amine terminal anchor or fluorine or methyl substitutions at the terminal para position. However, a low conductance state is observed in all amino-*p*-terphenyl derivatives with one preinstalled anchor due to molecular junctions formed by noncovalent dimeric $\pi-\pi$ stacking interactions. The observed high conductance state diminishes upon the addition of reducing agents and is restored upon the addition of an oxidizing agent. Our results suggest that the high conductance state arises due to Au−C(sp^2) bond formation facilitated by a single electron oxidation event at the electrode surface. A series of control experiments with different anchor groups shows that primary amines play a key role in forming Au−C bonds for molecular junctions. Overall, these results suggest that Au−C bond formation gives rise to high conductance pathways in organic molecules containing only one preinstalled terminal anchor. Insights from this work can be leveraged in the design of molecular electronic devices, particularly in understanding the mechanisms of molecular binding and junction formation.

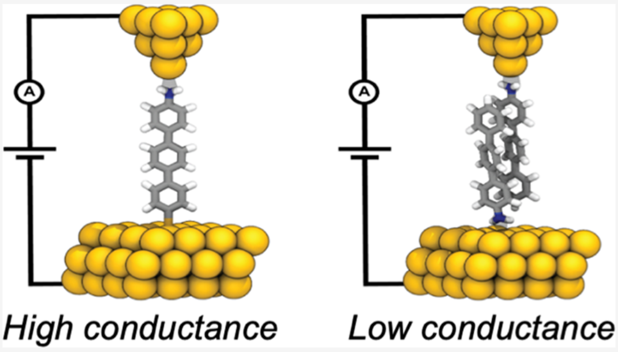

■ INTRODUCTION

Molecular junctions generally consist of three main components: a molecular bridge,[1] metal electrodes,[2] and terminal anchor groups that electronically couple the bridge to the electrodes.[3−6] Terminal anchors[3−5] play a key role in controlling the electronic properties of single molecule junctions via molecular binding, junction stability, and electronic coupling. One class of robust terminal anchors is characterized by dative bonding interactions with metal electrodes, including amine,[6,7] thiol,[8] pyridine,[9] and methyl thiol[10] groups. However, molecular junctions generally require two preinstalled terminal anchor groups to form a closed circuit, which poses synthetic challenges that tend to restrict the chemical space for molecular junction design. From this view, new binding modalities that avoid the requirement of two preinstalled terminal anchors could expand the scope of the chemical toolbox available for molecular electronics.

In addition to dative anchor groups, Au−C covalent anchors have been reported to yield stable and highly conductive molecular junctions.[11] Au−C(sp^2) contacts are generally found to be less conductive than benzyl Au−C(sp^3) contacts, likely due to the misalignment of Au−C(sp^2) bonds with the backbone π-system. The properties of covalent anchors directly affect electron transport, highlighting challenges in achieving robust and well-defined electronic pathways in molecular junctions using covalent contacts.[12] Direct formation of Au−C covalent bonds in molecular junctions typically requires cleavage or reaction of functional groups such as iodine,[13]

Received: September 1, 2025
Revised: September 12, 2025
Accepted: September 15, 2025
Published: September 20, 2025

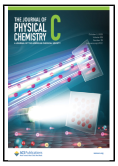

https://doi.org/10.1021/acs.jpcc.5c06124
J. Phys. Chem. C 2025, 129, 17458−17471

alkyne,[14,15] or diazonium[16,17] to generate Au−C bonds through in situ reactions. Recently, oriented external electric fields[18,19] have gained increasing attention for their ability to reorganize the electron distribution of molecules, stabilize charge-separated resonant forms, and promote chemical reactions.[20] Prior work suggests that it may be possible to form new types of anchors in nanoscale junctions under external electric fields, for example using C−H activation or electrochemical radical substitution reactions.[14] However, the structural and electronic properties that promote the formation of Au−C contacts under external electric fields are not yet fully understood.

Singly anchored molecules lack a second terminal anchor group to complete a closed electronic circuit. Prior work has reported that electron transport in singly anchored molecules occurs by noncovalent interactions such as $\pi-\pi$ stacking[21,22] and Au-π interactions.[23] However, the unanchored terminus is exposed to a strong electric field in the nanogap between electrodes, which could give rise to an electrochemically driven redox event or provide enhanced stabilization of polar or charged resonance states of the molecule. In this way, the nanogap environment could promote covalent bond formation,[13,17] giving rise to dual-tethered molecular junctions in molecular backbones without the need for conventional preinstalled anchors. In addition, understanding the electron transport behavior in π-conjugated molecules with one terminal anchor group could provide additional insights into noncovalent intermolecular interactions. Intermolecular charge transport[24] in π-stacked aromatic groups is critical to organic electronics.[25] The efficiency of electron transport in π-stacked systems depends on the electronic coupling and the distance and orientation between neighboring π-stacked molecules.[26−28] Although recent work has examined electron transport in singly anchored organic molecules,[22,29,30] we lack a comprehensive understanding of the behavior of singly anchored molecules in molecular junctions, particularly regarding how specific structural or electronic features influence charge transport properties and pathways.

In this work, we investigate the electron transport behavior of *p*-terphenyl derivatives containing one preinstalled anchor using a combination of automated chemical synthesis, single molecule electronics experiments, molecular dynamics (MD) simulations, bulk electrochemistry and spectroscopy, and nonequilibrium Green's function−density functional theory (NEGF−DFT) calculations. Synthesis of *p*-terphenyl derivatives was performed using a rapid Suzuki−Miyaura cross coupling (SMCC) method with reduced reaction time and temperature.[31] Following chemical synthesis and characterization, the electronic properties of these molecules were characterized using the scanning tunneling microscope−break junction (STM−BJ) technique.[32,33] Our results show that 4-amino-*p*-terphenyl (PPP) and related analogs have a surprisingly well-defined high conductance feature despite the presence of only one preinstalled terminal anchor. Our results further reveal a low conductance feature for all singly anchored amino-*p*-terphenyl derivatives studied in this work, which arises due to noncovalent intermolecular interactions. Flicker noise analysis and machine learning methods such as correlation 2D analysis and Gaussian mixture modeling (GMM) are used to understand the conductance behavior. In addition, cyclic voltammetry (CV), bulk electrolysis, and spectroscopy were used to understand the origin of the high conductance state, which arises from Au−C bond formation due to a single electron oxidation event.[34] Broadly, our work shows that Au−C(sp^2) contacts in terphenyl junctions provide more highly conducting pathways than noncovalent intermolecular interactions, but generally have similar conductance values as terminal anchors with dative contacts (Au−NH_2).

■ METHODS

Chemical Synthesis. All reactions were carried out under an atmosphere of nitrogen or argon in flame-dried or oven-dried glassware with magnetic stirring unless otherwise indicated. Organic solutions were concentrated via rotary evaporation under reduced pressure with a bath temperature of 50 °C unless otherwise noted. Normal phase flash column chromatography was performed using Merck silica gel grade 9385 60 Å (230−400 mesh) and a Biotage Selekt medium pressure liquid chromatography (MPLC) instrument. Small molecule synthesis was performed on an automated modular small molecule synthesizer (Supporting Information Sections S2−S4 and Figures S3−S19), as previously reported.[35]

Chemical Characterization. *NMR.* ^1H NMR and ^{13}C NMR spectra were recorded on Carver B500, or Bruker 600 NEO instruments. ^{11}B-NMR and ^{19}F NMR were recorded on a Carver B500 spectrometer. Chemical shifts (δ) are reported in parts per million (ppm) downfield from tetramethylsilane and referenced to residual protium in the NMR solvent ($CDCl_3$, δ = 7.26; acetone-d_6, δ = 2.05, center line). Data are reported as follows: chemical shift, multiplicity (s = singlet, d = doublet, t = triplet, q = quartet, quint = quintet, sept = septet, m = multiplet, b = broad), coupling constant (J) in Hertz (Hz), and integration. Chemical shifts (δ) for ^{13}C NMR are reported in ppm downfield from tetramethylsilane and referenced to carbon resonances in the NMR solvent (CDCl3, δ = 77.0, center line; acetone-d_6, δ = 29.8, center line). Carbons bearing boron substituents were not observed (quadrupolar relaxation).

Mass Spectrometry. High resolution ESI mass spectra were recorded on a Micromass 70-VSE spectrometer, Micromass Q-TOF Ultima spectrometer, Agilent 6530C QTOF, Autoflex Speed LRF, and an UltrafleXtreme TOFTOF.

Single-Molecule Conductance Measurements. Single-molecule conductance measurements were performed using a custom−built scanning tunneling microscope break junction (STM−BJ), as previously reported.[32,33,36] Gold substrates were prepared by evaporating 100 nm of gold onto polished Ted Pella AFM specimen disks with an e-beam evaporator. STM tips were prepared with 0.25 mm Au wire (99.998%, Alfa Aesar). Measurements were performed in 1,2,4-tricholorbenzene (TCB) and propylene carbonate (PC) solvents. For the measurements carried out in PC solvent, the STM tips were coated with Apiezon wax to minimize the exposed area to polar solvents and to reduce the non-Faradaic current. During experiments, the STM tip is controlled by a piezoelectric micropositioner to repeatedly form and break molecular junctions, and the current was recorded and analyzed during this process. A variable-gain low noise current amplifier (DLPCA-200 from Artisan Technology Group) was used to accurately convert current to voltage for data processing. Conductance histograms (determined from >5000 individual molecules per experiment) are generated for all molecules without data selection.

Temperature-dependent STM-BJ measurements were performed by heating the substrate with a thermistor. The heating unit was electronically shielded to avoid electromagnetic interference generated by local instrument electronic noise. The substrate temperature was modulated by a TC-720 temperature controller. Before each measurement, the STM-BJ setup was set at the desired temperature for sufficient time such that the temperature variation during the measurement was maintained to within 0.1 °C. To minimize the effect of solvent evaporation during measurements, STM-BJ experiments were performed in an airtight chamber such that a saturated chamber atmosphere effectively limited the solvent evaporation rate. The approximate chamber volume is 3.4 L. It should also be noted that the boiling point of 1,2,4-trichlorobenzene (TCB) is 213.5 °C, which is significantly higher than the temperature at which the experiment was conducted.

Correlation Analysis and Machine Learning. *Correlation 2D Analysis.* Correlation 2D analysis[37] is used to understand the statistical relations between distinct junction features. This analysis technique is often used to obtain information about junction conformations with different conductance values. This statistical analysis method is based on two-dimensional cross-correlation histogram (2DCH). A 2D covariance histogram is constructed, correlations are used to determine if the two-conductance states are occurring independently (negatively correlated, depicted in magenta) or sequentially (positively correlated, depicted in green) in a single molecule conductance trace.

Gaussian Mixture Modeling. Unsupervised learning algorithms (such as K-means++[38] and spectral clustering analysis[39]) were used to analyze single molecule conductance data. To understand the bimodal conductance distribution observed for the class of 4-amino-*p*-terphenyl molecules, we employ a classification algorithm for data clustering based on Gaussian mixture modeling (GMM). GMM offers advantages over alternative methods such as K-means due to its ability to detect subpopulations of unequal covariance. Clustering is carried out using 1D and 2D conductance histograms. From each individual trace, a 30-by-30 two-dimensional histogram and a 100-bin one-dimensional histogram are determined. These are combined to form a 1000-dimensional feature space ($30 \times 30 + 100$) over which GMM operates. The classification operates on the conductance range of 0 to $-5.5 \log(G/G_o)$, and displacement range of −0.1 to 1 nm (0 nm corresponds to the point where the junction gets broken, the −0.1 to 0 nm regime indicates metal−metal contact. All traces are aligned at 0.5 G_o as the starting point of displacement).

Flicker Noise Analysis. Flicker noise analysis was performed to differentiate between through-bond and through-space electron transport modes. To perform this analysis, the conductance fluctuations were experimentally determined while holding molecular junctions at a fixed tip-to-substrate separation for 150 ms. The transient conductance response is then analyzed using discrete Fourier transform to obtain the noise power spectral density (PSD). Flicker noise power is determined by numerically integrating the PSD between frequencies of 100 to 1000 Hz. 2D flicker noise histograms are then determined based on the flicker noise power and their corresponding average conductance. The relationship between the noise power and the average conductance can be described based on a scaling factor n. By fitting the 2D flicker noise histogram with a 2D Gaussian, the scaling factor n is determined when the correlation between the noise power/G^n and the average conductance is minimized. A scaling factor of $n \approx 1$ indicates through-bond conductance, whereas a scaling factor of $n \approx 2$ indicates through-space conductance.

Bulk Electrochemical Experiments. We performed bulk electrochemical experiments[40] to gain an understanding of the redox behavior of 4-amino-*p*-terphenyl (PPP). Bulk electrochemical experiments were carried out using a CHI760E bipotentiostat. Cyclic voltammetry (CV) was performed using a 3 mm diameter gold disk as working electrode, a carbon rod as a counter electrode, and an Ag/AgCl (3.0 M KCl) reference electrode with a salt bridge. CV was performed on a 1 mM solution of PPP in a supporting electrolyte solution of 0.1 M tetrabutylammonium hexafluorophosphate ($TBAPF_6$) in propylene carbonate. CVs were performed at a range of scan rates from 25 mV/s up to 1 V/s, scanning from 0.0 V vs Ag/AgCl to either 0.8 or 1.0 V vs Ag/AgCl. All cyclic voltammetry data is reported in IUPAC convention and performed without applying *iR* compensation.

Bulk electrolysis experiments were carried out in either H-cells or W-cells for preparative or quantitative bulk electrolysis experiments, respectively. The H-cell consisted of two compartments separated by a glass-frit, with one compartment for the working and reference electrode and the other compartment for the counter electrode. The W-cell consisted of three compartments separated by glass frits, with the center compartment containing the working electrode, and the two neighboring compartments containing the reference or counter electrode. Electrolysis in the H-cell and W-cell used, respectively, 20 and 5 mL of 1 mM 4-ATP in $TBAPF_6$/PC electrolyte system. Reticulated vitreous carbon foam was used as the working electrode and counter electrode, and Ag/AgCl electrode with a salt bridge was used as a reference electrode. All electrolysis experiments were carried out at a constant potential of 0.8 V vs Ag/AgCl and the potential was applied until the current reached 1% of the initial electrolysis current. Bulk electrolysis was carried out while bubbling argon into solution. Integrated charge values recorded by the potentiostat were used to determine the number of electrons transferred.

Preparative electrolysis was performed using an H-cell to obtain electrolysis product for further workup and analysis. Electrolysis products were removed from the H-cell and used for further analysis. An extraction was performed to remove solvent and electrolyte from the bulk electrolysis products.[41] Twenty mL of the electrolyzed PPP in $TBAPF_6$/PC electrolyte was added to a separatory funnel, along with 20 mL of diethyl ether. The mixture was first washed with 20 mL of brine, followed by washing twice with 20 mL of water. The organic layer was dried over magnesium sulfate and filtered into a round-bottom flask. The organic extraction products were placed on a rotary evaporator for 3 h with a bath temperature of 70 °C and a vacuum pressure of 30 mbar. The final volume after evaporation was approximately 5 mL.

Electron Spin Resonance Spectroscopy Experiments. ESR measurements were performed by aliquoting the electrolyzed or control solution into a quartz capillary within a 4 mm thin-walled precision quartz EPR tube (Wilmad). The solvent was propylene carbonate (PC). Spectra were acquired at room temperature (298 K) with a Bruker EMXPlus X-band instrument. Measurement conditions were 3600 G center field, 8 scans, 20 mW microwave power, 2.0×10^3 gain, 1 G modulation amplitude, 100 kHz modulation frequency, and a microwave frequency of ∼9.7775 GHz.

In Situ Surface Enhanced Raman Spectroscopy. A He/Ne 632.8 nm laser was used as the excitation source for

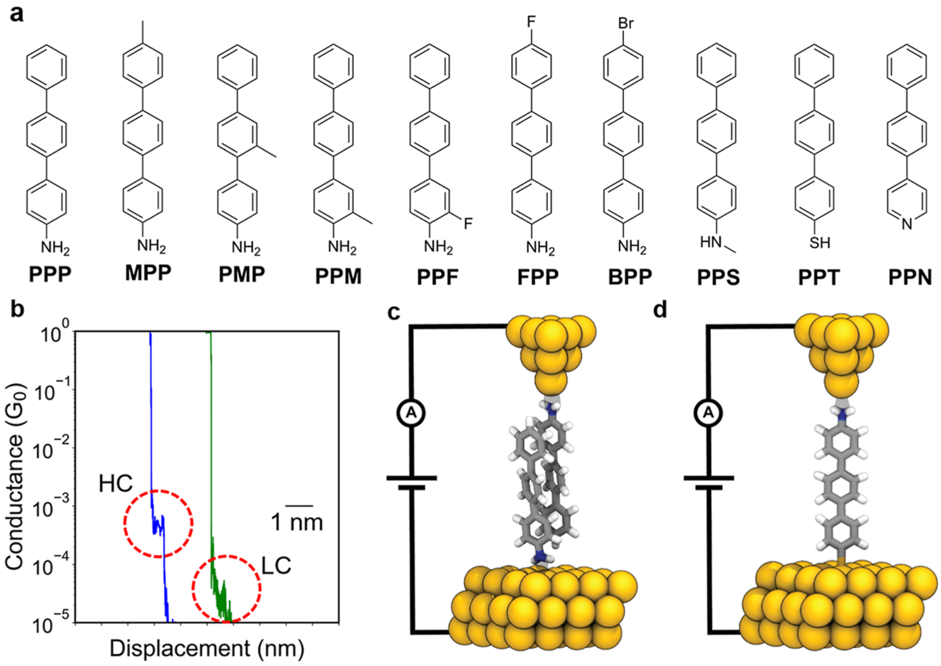

Figure 1. Molecular library and electron transport mechanisms for singly anchored terphenyl derivatives. (a) Structures of singly anchored organic molecules studied in this work. (b) Characteristic single molecule conductance traces observed in STM-BJ experiments for PPP. HC denotes the high conductance state, whereas LC denotes the low conductance state. (c) Molecular junction schematic with noncovalent dimeric interactions for PPP. (d) Molecular junction schematic featuring an Au−C bond for PPP.

SERS experiments. Spectra were accumulated from 30 individual acquisitions for 1 s each. For the potential sweep experiments, spectra were collected over a 30 s potential step while performing staircase voltammetry. Voltammetry performed during the SERS measurements was performed using a CHI760E potentiostat and a custom glass/Kel-F spectroelectrochemical cell.[42] The working electrode was a polycrystalline gold disk that was electrochemically roughened prior to the experiment.

Molecular Dynamics Simulations. For each terphenyl derivative, a pair of molecules was simulated in trichlorobenzene (TCB) and propylene carbonate (PC) solvent mediums, and their separation distance between the center-of-mass (COM) was systematically varied to provide molecular insights from both energetic and conformational perspectives. Energetically, the potential mean force (PMF) as a function of the separating distance between the COM of terphenyl pairs in the solution state was assessed using umbrella sampling and the Weighted Histogram Analysis Method (WHAM).[43] The error bars of the PMFs were obtained by Monte Carlo bootstrap error analysis. The force field parameters for the four terphenyl compounds and the two solvent species were specified using the optimized potentials for liquid simulations (OPLS)-AA force field,[44] and CM1A atomic partial charge,[45] obtained via the LigParGen web server.[46] In each terphenyl system, a pair of terphenyl molecules was placed at the center of the box, with their COM separated along the $\pi-\pi$ stacking director at a distance of 3.3 Å. Subsequently, 1600 solvent molecules were randomly added using PACKMOL.[47] Each initial MD configuration, with the dimer coordinates fixed, underwent equilibration for 100 ns at 300 K and 1 bar using the *NPT* ensemble, with a coupling constant of 0.1 ps for both the thermostat and barostat. The equations of motion were integrated using the velocity Verlet algorithm with a time step of 1 fs, and periodic boundary conditions were applied in all three dimensions. Long-range electrostatic interactions were computed using the particle−particle particle-mesh Ewald technique with a precision of 0.0001, and a real space cutoff of 15 Å was set. The same cutoff distance was employed to truncate Lennard-Jones interactions, and geometric mixing rules were applied for different atom pairs. The MD simulations were performed using LAMMPS.[48]

For each terphenyl dimer solution, utilizing equilibrated configurations, we conducted a series of 30 MD simulations with an external harmonic constraint applied between the COM of the dimer. The constrained COM distance ranged from 3.3 Å to 9.1 Å, with intervals of 0.2 Å, and a harmonic force constant of 100 kcal/mol was used to restrain the dimer at the correct constrained COM distance. Each simulation window underwent 1 ns of equilibration under the *NPT* ensemble at 300 K and 1 bar, followed by an additional 4 ns of simulation to capture pair conformations at a frequency of 1 ps. The pair conformations collected from the 30 MD windows were used to estimate the PMF through the WHAM.

Nonequilibrium Green's Function-Density Functional Theory. NEGF-DFT calculations are performed with a DFT-based nonequilibrium Green's function (NEGF) approach using the TranSiesta and Tbtrans package.[49−51] The electrodes contain 8 layers of 16 gold atoms along with a pyramid of 10 Au atoms. The amines on the singly anchored amino-*p*-terphenyl derivatives were made to interact with the gold atoms in an antiparallel configuration. The high conductance state of PPP was represented using an amine and carbon atom as two anchoring sites. Geometry relaxation of the sequences was performed using generalized gradient approximation−Perdew−Burke−Ernzerhof (GGA−PBE) functional[52] using the TranSiesta package.[50] SZP or DZ basis sets were used for all the gold atoms. DZP basis sets were used for carbon, hydrogen, and nitrogen. Electrode calculations were carried out with a 4 × 4 × 50 k-mesh. The geometry relaxation was carried out using a 4 × 4 × 1 k-mesh, which was performed until the forces were <0.05 eV/Å. After the junction was relaxed, the transport calculations were carried out using the TranSiesta package[49,51] with the same functionals, basis sets, pseudopotential, and k-mesh as the geometry relaxation. Convergence was tested prior to transmission calculations, using a real axis integration internal from −40 eV to infinity;[49] this includes a crossing in the imaginary axis at 2.5 eV, and the γ value is $-10\ k_BT$. The circle grid consists of 102 G-Legendre points, and 15 G-Fermi points for the tail portion. Tbtrans[51] was used to carry out the NEGF calculations and to obtain electron transmission as a function of energy (relative to the Fermi energy level). NEGF calculations were carried out from −3 to 3 eV with 0.01 eV energy increments.

RESULTS AND DISCUSSION

Chemical Synthesis and Characterization. Synthesis of several organic molecules was carried out using Suzuki−Miyaura cross coupling (SMCC) by leveraging recent advances in iterative automated synthesis.[31] Prior SMCC conditions for automated synthesis require more than 12 h to prepare one molecule,[53] and manual synthesis requires even longer time scales to synthesize a library of small molecules.[35,54,55] In this work, we used automated iterative coupling[35,53] based on a new rapid SMCC method (Supporting Information Sections S3 and S4) that significantly decreases the reaction time to 10 min with high yield.[31]

An automated small molecule synthesizer (Figure S3a) capable of parallel runs of deprotections, couplings, and purifications was used, as previously reported.[53] The building blocks and protecting groups used in the reaction are shown in Figure S3b. The synthesis of 4″-methyl-[1,1′:4′,1″-terphenyl]-4-amine (MPP), 3-fluoro-[1,1′:4′,1″-terphenyl]-4-amine (PPF), *N*-methyl-[1,1′:4′,1″-terphenyl]-4-amine (PPS), 4″-fluoro-[1,1′:4′,1″-terphenyl]-4-amine (FPP), 4″-bromo-[1,1′:4′,1″-terphenyl]-4-amine (BPP), and 4-([1,1′-biphenyl]-4-yl) pyridine (PPN) was carried out using one step slow release SMCC chemistry (Figure S3c). 2′-methyl-[1,1′:4′,1″-terphenyl]-4-amine (PMP) and 3-methyl-[1,1′:4′,1″-terphenyl]-4-amine (PPM) were synthesized using a two-step synthesis process: rapid SMCC followed by slow release SMCC (Figure S3d). [1,1′-biphenyl]-4-amine (PP), [1,1′:4′,1″-terphenyl]-4-amine (PPP), [1,1′:4′,1″-terphenyl]-4,4″-diamine (ADP), and 1,1′,4′,1″-terphenyl-4-thiol (PPT) were purchased from commercial sources. Mass spectrometry and ^{1}H and ^{13}C nuclear magnetic resonance (NMR) spectrometry were used to characterize molecules prior to electronics experiments (Supporting Information Section S1−S4, Figures S1, S2 and S4−S19).

In this work, the chemical space focuses on *p*-terphenyl derivatives for molecular electronics due to their rigidity and extended π-conjugation, which results in low tunneling barriers.[56−59] We designed a series of *p*-terphenyl molecules with one preinstalled anchor (Figure 1a) based on the parent molecule PPP by including additional substituents on the three benzene rings. PPM, PMP, and MPP each contain a methyl group on one of the aromatic rings, which changes preferred resonance structures, alters ring torsional angles, or introduces steric hindrance during the formation of molecular junctions. Molecule PPF was incorporated to investigate the effect of electron withdrawing groups in contrast to the electron donating nature of the methyl substituted terphenyls. Furthermore, BPP and FPP were synthesized as additional control molecules for understanding the electron transport mechanism in terphenyl derivatives. Three additional control molecules, PPN, PPS, and PPT, are characterized to understand the role of anchor groups.

Single Molecule Conductance Measurements. The electronic properties of *p*-terphenyl derivatives were characterized at the single molecule level using the scanning tunneling microscope-break junction (STM-BJ) technique.[32,33] The STM-BJ setup consists of a gold tip electrode that is repeatedly moved into and out of contact with a gold substrate electrode in a solution containing molecules, resulting in the continual formation and breakage of single molecule junctions. The STM-BJ instrument is automated, and experiments are repeated over an ensemble of >5000 molecules for each experiment. Single molecule conductance data are then analyzed using one- and two-dimensional (1D and 2D) conductance histograms without data selection. In 1D conductance histograms, all recorded conductance values over the course of the measurement are compiled. The peak of the histogram represents the most probable conductance value for a given molecule. 2D molecular conductance histograms show the distribution of conductance values together with junction separation distances, providing insights into the evolution of conductance as the junction is extended. The time scale of a single STM- BJ pulling trajectory is in the order of milliseconds,[60] which allows for sampling a range of molecular conformations[61] during a conductance measurement.

We began by characterizing the electron transport behavior of PPP ([1,1′:4′,1″-terphenyl]-4-amine) and ADP ([1,1′:4′,1″-terphenyl]-4,4″-diamine). Our results show that PPP has a high conductance state at $\sim 10^{-3.28}\ G_0$ and a low conductance state at $\sim 10^{-4.78}\ G_0$ (Figure 1b), whereas ADP has a high conductance state at $\sim 10^{-3.41}\ G_0$ and low conductance state at $\sim 10^{-4.66}\ G_0$ (Figures S20 and 21). A comparison of the full width at half maxima (fwhm) for PPP and ADP (Figure S22) suggests the possibility of forming a robust electronic pathway for molecules with a single preinstalled terminal anchor (PPP) compared to those with two preinstalled anchors (ADP).

Characteristic single molecule conductance traces for PPP show high and low conductance features in separate and distinct molecular subpopulations (Figure 1b). Singly anchored molecules are generally thought to form junctions through intermolecular stacking interactions,[21,22] where two different molecules, each anchored to a different electrode, form noncovalent dimeric interactions to complete the circuit. We hypothesized that the low-conductance feature in singly anchored *p*-terphenyl derivatives arises due to intermolecular stacked junctions (Figure 1c). In contrast, the high-conductance feature observed for PPP is a robust and well-defined electronic pathway that cannot arise due to noncovalent intermolecular interactions. In the STM-BJ setup, the applied bias between the two electrodes results in relatively high electric field gradients (∼0.1−0.5 V/nm) in the nanoscale junction. We posited that the electric field could promote the formation of a new covalent anchor in molecular junctions (Figure 1d). We aimed to understand if such a mechanism could give rise to a new terminal anchor and well-defined[62] conductance pathways in molecules with only one preinstalled terminal anchor.

We characterized the electron transport properties of several amino-*p*-terphenyl derivatives in nonpolar solvents (1,2,4-trichlorobenzene, TCB) using the STM-BJ method (Figure 2).

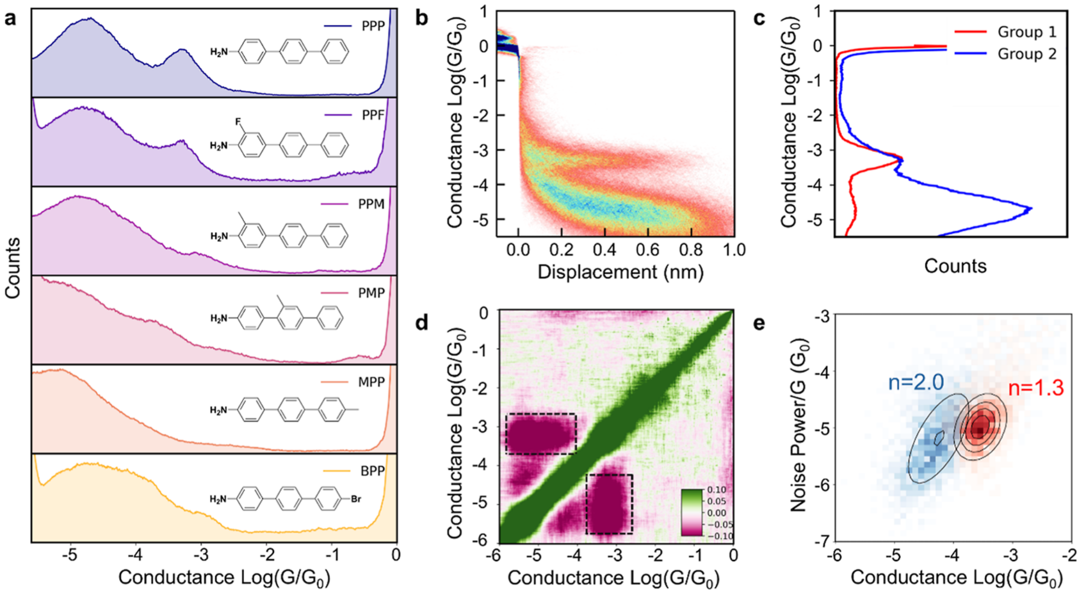

Figure 2. Scanning tunneling microscope-break junction (STM−BJ) measurements of amino-*p*-terphenyl derivatives in 1,2,4-trichlorobenzene (TCB) at 250 mV applied bias. (a) 1D conductance histograms for PPP, PPM, PMP, and MPP. (b) 2D conductance histogram for PPP. (c,d) Gaussian mixture modeling and 2D correlation analysis on PPP revealing anticorrelated high and low conductance states. (e) Flicker noise analysis of molecular subpopulations corresponding to the high and low conductance feature for PPP, which suggests through-bond and through-space characteristics for the high and low conductance features (scaling exponents of $n \approx 1.3$ and $n \approx 2$, respectively).

Our results show that all amino-*p*-terphenyl derivatives with a single preinstalled anchor exhibit a characteristic low conductance feature (Figures 2a and S23). PPP shows an additional high conductance feature occurring in a significant molecular subpopulation over a large ensemble of molecules (Figure 2b). Moreover, this high conductance feature is also present in several amino-*p*-terphenyl analogs such as PPF (Figures 2a and S23a), though diminished in comparison to PPP.

Unsupervised machine learning, 2D correlation analysis, and Gaussian mixture modeling (GMM), were used to interpret the two-state conductance behavior observed for PPP. Bimodal conductance distributions can arise due to conformationally distinct molecular subpopulations that do not interchange during molecular pulling events (static heterogeneity) or due to conformation-dependent conductance states that occur during molecular pulling events (dynamic heterogeneity).[61] Gaussian mixture model (GMM) clustering was performed for PPP to identify and separate the two conductance features. Results from cluster analysis were then plotted and analyzed (Figure 2c), revealing that two distinct clusters correspond to the high- and low-conductance features, which is consistent with static heterogeneity or conformationally distinct molecular junctions. 2D correlation analysis and GMM indicate that the two conductance states of PPP are negatively correlated and therefore occur independently in distinct trajectories during the STM-BJ experiments (Figure 2d).[6] Compared to PPP, GMM clustering for ADP did not reveal any distinct patterns, suggesting differences in electron transport behavior between PPP and ADP (Figure S24).

Flicker noise analysis[63] was performed to differentiate between through-bond and through-space electron transport for the high and the low conductance states. Prior work has shown that the conductance fluctuations (conductance noise power) exhibit a power law dependence on the mean conductance G values depending on through-space and through-bond transport characteristics.[6,64] Conductance noise is quantified by numerically integrating the conductance noise power spectral density (PSD) between frequencies of 100 and 1000 Hz.[24,63] The correlation is quantified by the scaling exponent n of the normalized noise power (noise power/G^n) versus the average normalized conductance G/G_0, where G_0 is the conductance quantum. A scaling exponent $n \approx 2$ suggests through-space transmission whereas an exponent $n \approx 1$ corresponds to through-bond transport. These results show that the low conductance state in PPP occurs by through-space electron transport, whereas the high conductance state shows dominant through-bond electron transport characteristics (Figure 2e). Flicker noise analysis for MPP (Figure S25) is also consistent with through-space electron transport for the low conductance state. Based on these results, the low conductance state observed for all amino-*p*-terphenyl derivatives likely arises due to noncovalent dimeric interactions. We posit that the high conductance state in PPP arises due to the formation of a new covalent anchor binding to the metal electrode, which is consistent with through-bond transport for the high conductance state. Based on the structure of PPP and results from bulk spectroscopy and electrochemistry characterization (vide infra), we hypothesize that the second anchor involves the formation of an Au−C bond (Figure 1d) via an electrochemical radical substitution reaction.

2D conductance histograms for amino-*p*-terphenyl derivatives indicate stark differences in electron transport pathways for different molecular compositions. Notably, the high conductance state observed in PPP is diminished in PPF, PPM, and PMP, suggesting that molecular substituents inhibit the high conductance pathway in these terphenyl backbones (Figures 2a and S23). The high conductance feature is completely absent in MPP, implying that the presence of a methyl group at the para position on the aromatic ring abolishes the high conductance pathway. We also characterized the electron transport behavior of BPP and FPP which contain

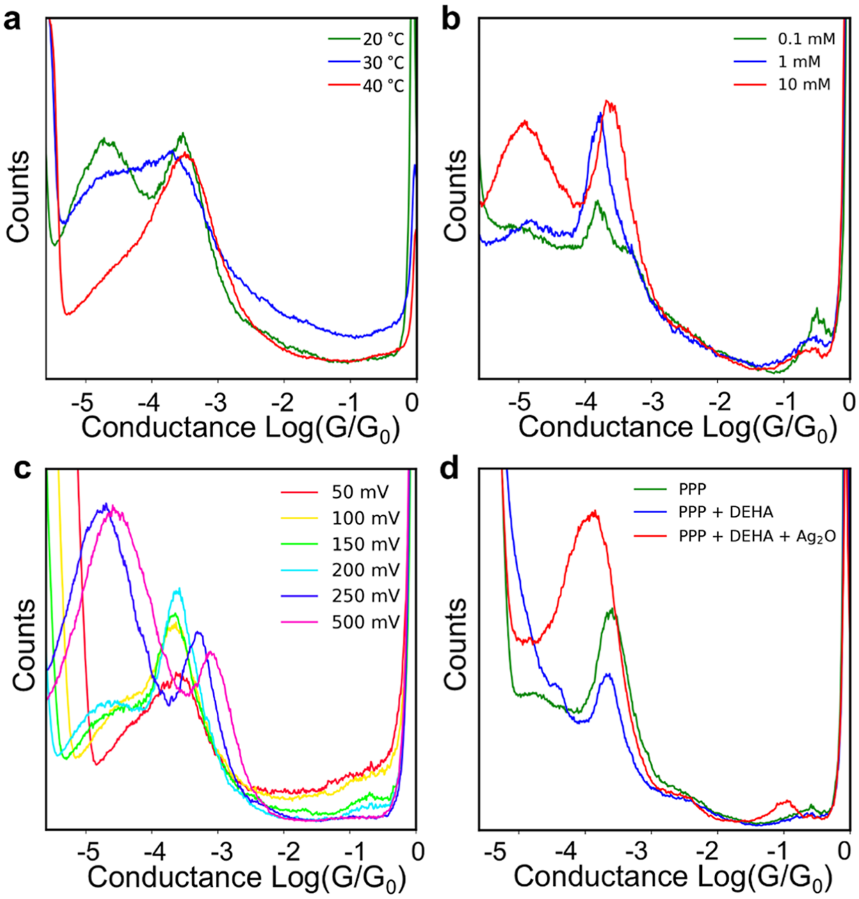

Figure 3. Effect of temperature, concentration, applied bias, oxidizing and reducing agents on the molecular conductance of PPP. (a) Temperature-dependent conductance measurements are consistent with noncovalent dimeric interactions for low conductance state, whereas the high conductance state is robust to temperature variations. (b) Concentration-dependent measurements for PPP. (c) Bias-dependent STM−BJ experiments indicating that the high conductance state is observed at low bias, whereas the low conductance state has bias dependence. (d) Reducing agent (DEHA) diminishes the high conductance state for PPP, and oxidizing agent (silver oxide) restores the high conductance state.

bromine and fluorine groups, respectively, at the para position on the phenyl ring farthest from the terminal amine anchor (Figures 2a and S26). These results show that the high conductance state is completely abolished in FPP and nearly absent in BPP.

Based on these results, we hypothesized that the carbon atom at the terminal para position in amino-*p*-terphenyl derivatives such as PPP, PPM, and PMP forms an Au−C covalent bond due to an oxidation event at the metal electrode, leading to the formation of a terminal covalent anchor that completes the circuit and gives rise to the high conductance state (Figure 1d). The absence of the high conductance feature in MPP and FPP is consistent with the hypothesis that a methyl or fluorine group at the terminal para position inhibits the interaction between the molecule and the gold electrode, preventing the formation of the Au−C linkage. However, the para position remains available for binding in the amino-*p*-terphenyl derivatives PPM and PMP. PMP contains a methyl substituent on the central ring, which alters the torsional angles and could inhibit the stability of resonance structures during electrochemical oxidation, resulting in a weak high conductance feature compared to PPP.

Prior work has focused on 4″-iodo-[1,1′:4′,1″-terphenyl]-4-yl)(methyl)sulfane (IPS),[13] which contains thiomethyl and aryl iodide at the terminal positions of a terphenyl molecule. PPP exhibits different electron transport characteristics compared to IPS due to differences in anchor−gold binding (amine versus thiomethyl anchors) and the functional group at the other end of the molecule (−H versus −I). To understand the role of terminal anchors, we characterized the electronic properties of PPN, PPT, and PPS that contain thiol, pyridine, and *N*-methylamino as terminal anchor groups, respectively (Figure S27). Our results show that the high-conductance state is absent in PPN, PPT, and PPS. PPN exhibits a low conductance state that is absent or significantly diminished in PPT and PPS and likely arises due to noncovalent dimeric interactions. These results show that the amine anchor is critical for the formation of Au−C linkage in terphenyl junctions.

We also characterized the electron transport behavior of [1,1′-biphenyl]-4-amine (PP) (Figure S28). Our results show a bimodal conductance distribution for PP, with a weak high-conductance feature consistent with Au−C bond formation. Taken together, these results suggest that the presence of an amine anchor on a *p*-phenyl backbone is crucial for the formation of Au−C linkages.

Temperature-dependent STM-BJ measurements were performed at three different temperatures: 20 °C, 30 and 40 °C. Increased temperature leads to enhanced molecular vibrations, reducing the likelihood of forming intermolecular junctions during the STM−BJ experiments.[65] Our results indicate that as the temperature is increased, the low conductance state is

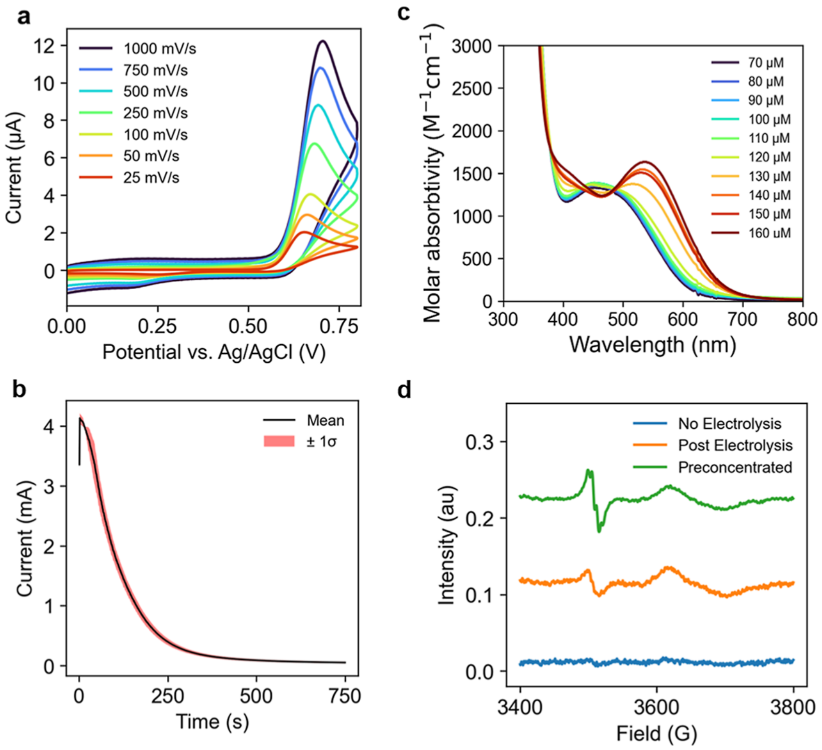

Figure 4. Bulk electrochemistry and spectroscopy experiments on PPP. (a) Cyclic voltammetry of 1 mM PPP in an electrolyte solution of 0.1 M TBAPF$_6$ in PC. The potential was swept from 0 V vs Ag/AgCl to 0.8 V vs Ag/AgCl in forward and reverse scans at rates ranging from 25 mV/s up to 1 V/s. (b) Bulk electrolysis of 1 mM PPP in an electrolyte solution of 0.1 M TBAPF6 in PC, at an applied potential of 0.8 V, taken in triplicate ($N = 3$). The black trace indicates the mean, and the red error bar represents 1 standard deviation from the mean. The average number of electrons transferred was 1.1 ± 0.1. (c) UV−vis spectra for oxidized PPP (post electrolysis) with increasing concentration. (d) Electron spin resonance (ESR) spectra of the 1 mM PPP with no electrolysis, directly after electrolysis, and after electrolysis with a preconcentration step.

significantly diminished (Figure 3a). These results are consistent with our hypothesis that the low conductance state arises due to noncovalent dimeric interactions. On the other hand, the high conductance state is largely unaffected by the 20 °C increase in temperature, which differs from the temperature-dependent electron transport behavior of ADP (Figure S29), suggesting the high conductance state arises due to stronger anchor binding for PPP compared to ADP. Concentration-dependent STM−BJ experiments were also performed for PPP in the range on 0.1−10 mM (Figure 3b). These results indicate that the low conductance state of PPP exhibits strong concentration dependence, whereas the high conductance state is concentration independent. These results further support our hypothesis that the low conductance state arises due to noncovalent dimeric interactions whereas the high conductance state arises due to through-bond transport.

Bias dependent STM−BJ experiments (Figure 3c) reveal that at low applied bias (50−150 mV), only the high conductance state is observed. As the applied bias is increased, the low conductance state emerges, consistent with prior work reporting that increased bias regulates dimeric interactions in molecular junctions.[30] Increasing bias can lead to stronger coupling at the Au−C linkage, leading to enhancement in conductance. To further investigate the electron transport behavior of PPP, we performed the STM-BJ experiments in the presence of reducing and oxidizing agents (Figures 3d, S30 and 31). Results from these experiments show that the high conductance state diminishes with an increase in the concentration of the reducing agent (*N*,*N*-diethylhydroxylamine or DEHA). However, the diminished high-conductance state can be fully restored upon the addition of an oxidizing agent (silver oxide) (Figures 3d and S32). Overall, these results indicate that the high conductance state observed for PPP can be chemically tuned through the application of reducing or oxidizing agents, suggesting that a redox event is responsible for the high conductance state.

The two-state conductance behavior of PPP is also observed in a polar solvent such as propylene carbonate (PC), but with lower counts for each molecular conductance subpopulation as the higher dielectric strength of polar solvents likely reduces the effect of the electric field (Figure S33).[19] We also characterized the molecular conductance of PPP in PC in the presence of a reducing agent (sodium borohydride, NaBH$_4$), which results in the disappearance of the high conductance state (Figure S34), consistent with the results observed in TCB. Overall, these results are consistent with electrochemical oxidation leading to Au−C bond formation and the high conductance state. Bulk electrochemistry, electrolysis, electron spin resonance, UV−vis spectroscopy, and surface enhanced Raman spectroscopy (SERS) were pursued to further understand the origin of the high conductance state.

Bulk Electrochemistry and Spectroscopy. Integrating single molecule measurements with bulk experiments offers a powerful approach to understand electron transport.[40,66] Here, we performed a series of bulk electrochemical and spectroscopy experiments to understand the electronic properties of amino-*p*-terphenyl molecules. Results from cyclic voltammetry (CV) experiments show a distinct oxidation wave on the forward scan at approximately 0.65 V versus Ag/AgCl, with

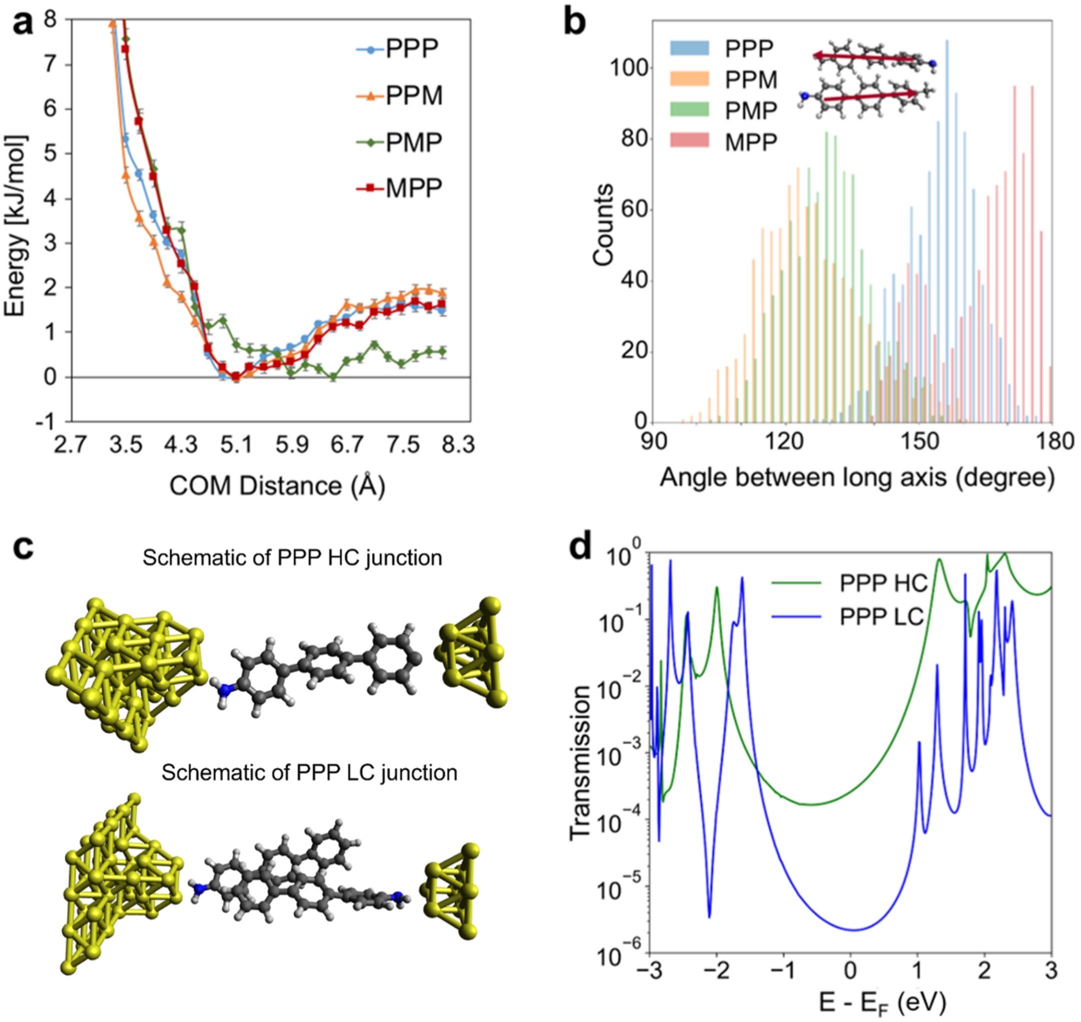

Figure 5. Molecular dynamics (MD) simulations and nonequilibrium Green's function-density functional theory (NEGF-DFT) calculations. (a) Potential mean force (PMF) profiles for dimers. (b) Distribution of the angle between the long axes of terphenyl molecules in 1,2,4-tricholorobenzene (TCB). Arrows in the inset represent the long-axis vector. (c) Schematic of molecular junctions comprised of PPP corresponding to the high conductance state (HC) and low conductance state (LC). (d) Transmission plots for HC and LC for PPP.

only a small reduction peak at 0.15 V on the return scan (Figure 4a). The absence of a prominent return peak in the CV indicates that a distinct chemical process occurs after oxidative electron transfer. A second distinct electron transfer event was observed when the positive limit of the potential window was expanded from 0.8 to 1.0 V, however this second electron transfer event leads to the formation of a surface-bound species (Figure S35). In situ electrochemical measurements were also performed using the STM-BJ setup by sweeping the voltage between the STM tip and bottom electrode, beginning with a ferrocene standard for internal calibration.[40] In situ CV experiments on PPP indicate that a redox reaction occurs during STM-BJ experiments (Figure S36). However, as previously reported, we note that it is challenging to quantitatively compare the potentials observed in bulk electrochemistry and STM-BJ experiments because the former setup relies on a three-electrode system and the latter is a two-electrode system.[50]

Bulk electrolysis was performed to understand the electrochemical oxidation of PPP (Figures 4b and S37). The potential was maintained at 0.8 V during electrolysis to isolate the first electron transfer event and avoid irreversible film formation on the electrode surface. All electrochemical experiments were performed in triplicates, and the integrated charge was used to determine the total number of electrons transferred during the electrochemical oxidation. Our results show that one electron is transferred during the oxidation event, which suggests that the electrochemical oxidation of PPP forms a radical cation species.

Based on results from bulk electrochemistry and single molecule experiments, we hypothesize that amino-*p*-terphenyl derivatives undergo a one-electron oxidation event, leading to a radical cation species that undergoes a substitution reaction at the para position (Figure S38). This reaction leads to the formation of an Au−C bond responsible for the high conductance state. These findings can be compared to prior work on electric field-driven electrophilic aromatic substitution reactions;[19] however, we note that the Au−C anchor formation mechanism in terphenyls such as PPP involves a one-electron oxidation reaction, whereas the electrophilic aromatic substitution reaction is not a redox-mediated chemical reaction.

We further conducted bulk spectroscopy experiments to understand the conductance behavior of PPP and related analogs. UV−vis absorption spectra of oxidized PPP post electrolysis clearly show a red shift with increasing concentration (Figures 4c and S39), suggesting the possibility of dimerization,[67,68] consistent with the enhanced low-conductance state at higher concentrations in single molecule electronic experiments. Electron spin resonance (ESR) spectroscopy experiments on PPP were also performed before electrolysis, after electrolysis, and after preconcentration of the electrolysis product, as shown in Figure 4d. The signals at ∼3480 G and ∼3650 G indicate the presence of a radical species in the electrolyzed solutions that is not present in the pre-electrolyzed sample, consistent with the proposed mechanism for the high conductance state.

We further performed surface-enhanced Raman spectroscopy (SERS) experiments on blank electrolyte (0.1 M $TBAPF_6$ in PC solvent), a terphenyl molecule without anchors, PPP, and FPP (Supporting Information Section S8, Figures S40, S41, Tables S1 and S2). Results from these experiments indicate that upon increasing the applied bias, a peak at 415 cm^{-1} appears for PPP, which is absent in terphenyl. For FPP, no peak at 415 cm^{-1} is observed up to an applied bias of 0.5 V, a result that is markedly different than PPP (Figure S40d). In SERS experiments, Au−C bonds[69] are typically characterized by peak values around 413−435 cm^{-1}, with prior literature reporting that Au−C bonds similar organic molecules appear at 415 cm^{-1}.[70] Nevertheless, we cannot exclude the possibility that this peak arises due to formation of an Au−N bond, though putative Au−NH_2 dative interactions are expected to occur even at zero applied bias. Finally, we note that the conditions in the in situ SERS experiment are drastically different than the STM−BJ experiments. The STM−BJ environment gives rise to strong electric field gradients (∼0.1−0.5 V/nm) in the nanogap, which likely promotes Au−C bond formation given the close proximity of the two adjacent gold electrodes.

Molecular Dynamics Simulations. MD simulations were used to characterize molecular geometries or conformations adopted by molecular junctions.[61] Here, we used MD simulations to characterize the noncovalent dimeric interactions that resemble the low conductance state observed in the single molecule experiments. A series of MD simulations was performed to elucidate the dimeric interactions between methyl substituted amino-*p*-terphenyl derivatives. For each terphenyl derivative, a pair of molecules was simulated in TCB and PC solvents, and the separation distance between their center-of-mass (COM) positions was systematically varied to provide molecular insights from both energetic and conformational perspectives.

The potential mean force (PMF) was assessed as a function of the separation distance between the COM of terphenyl pairs in solution using umbrella sampling and the weighted histogram analysis method (WHAM).[43] The PMFs of PPP, MPP, and PPM in TCB solution exhibit similar profiles, with the global minima located at a separation distance of 5.1 Å (Figure 5a). The corresponding binding energies (Table S3) between two terphenyl molecules is $0.63 \pm 0.04\ k_BT$ for PPP, $0.68 \pm 0.05\ k_BT$ for MPP, and $0.79 \pm 0.04\ k_BT$ for PPM, where T is the absolute temperature at 300 K. On the other hand, the global minimum of PMP is situated at a separation distance of 5.9 Å with a binding energy of $0.19 \pm 0.05\ k_BT$ due to the nonplanar intramolecular conformation and steric hindrance caused by its methyl group at the middle phenyl ring (Figure S42). The intermolecular binding energies for the terphenyl derivatives are below 1 k_BT, which is consistent with results from the temperature-dependent STM-BJ experiments for the low conductance state based on noncovalent dimeric interactions.

We further characterized the structural features of the terphenyl molecules based on the MD trajectories of the PMF global minimum. Figure 5b shows the angle distribution between the long axes of terphenyl molecules in TCB solvent, which quantifies the intermolecular structure between terphenyl dimers. An angle close to 180° indicates that the terphenyl molecules are aligned in the same parallel direction, increasing the likelihood of $\pi-\pi$ stacking and providing an efficient conductance pathway. For MPP, a bimodal distribution is observed which could arise due to the methyl group leading to an offset in stacking for the dimeric structure. The symmetric geometry of PPP in TCB promotes a more parallel pair structure, ensuring an effective stacked dimeric structure. A similar trend in PMFs and conformational features was observed for peptides in PC solution (Figure S43). Molecular conformations generated by MD are used in quantum mechanics (QM) calculations to aid in comparison between theory and experimental results for the dimeric state of the terphenyl derivatives studied in this work.

Electron Transport Calculations. Electron transport calculations provide a powerful tool to validate experimentally observed conductance behavior.[61,62] Nonequilibrium Green's function-density functional theory (NEGF−DFT) calculations were performed for junction conformations associated with the high- and low-conductance states. For the low conductance state, simulations were performed for methyl substituted amino-*p*-terphenyl derivatives in a stacked dimer geometry, corresponding to the low conductance state characterized by noncovalent intermolecular interactions. Computational transmission values (Table S4) corresponding to the low-conductance state of amino-*p*-terphenyl derivatives reveal that MPP exhibits lower electron transmission compared to the other derivatives. These results suggest that the presence of a methyl group at the terminal para position on the phenyl ring opposite to the amine can cause an offset in stacked molecular conformation. These results also support experimental results suggesting that the low conductance state arises due to noncovalent dimeric interactions.

Results from NEGF−DFT calculations reveal that the transmission calculations are qualitatively consistent with results from STM-BJ experiments, showing that the low conductance state has an approximately 10-fold smaller transmission probability compared to the high conductance state (Figures 5c,d and S44). Transmission calculations for the high-conductance state of PPP (Figure 5d), which involves the formation of an Au−C linkage, show electron transmission probabilities of 2.5×10^{-4} at the Fermi energy level, which is in good agreement with the experimentally observed conductance value of 5×10^{-4} from STM-BJ experiments. Overall, NEGF−DFT calculations combined with MD simulations support the hypothesis that the low conductance state arises due to noncovalent intermolecular interactions and the high conductance state involves the formation of a robust Au−C covalent linkage.

Finally, we calculated the oxidation energies of the terphenyl derivatives using DFT (Table S5). Our results show that the oxidation energies for the terphenyl molecules are approximately ∼6 eV, which is less than the applied bias being in the STM−BJ environment. However, the electric field gradients in the STM−BJ environment are larger than traditional bulk experimental setups,[34,71] which can trigger electric field-driven chemical reactions, as reported in prior work.[19] From this perspective, our work illustrates the possibility of observing electrochemical reactions in the STM−BJ environment, highlighting the importance of considering not only the applied bias but also the local electric field strength when interpreting redox activity in STM−BJ experiments.

■ CONCLUSIONS

In this work, the electronic properties of amino-*p*-terphenyl derivatives with one preinstalled anchor are characterized using automated chemical synthesis, single molecule electronics experiments, bulk electrochemistry, spectroscopy, MD simulations, and NEGF−DFT calculations. Single molecule experiments reveal two well-defined conductance states in several amino-*p*-terphenyl derivatives. Bulk electrochemistry and spectroscopy experiments show that a radical cation state occurs when PPP is exposed to an electric field, which facilitates the formation of robust Au−C covalent linkages due to an oxidation event. Our results show that the formation of Au−C linkages is favored when the stability of the charge separated resonance state is enhanced. The introduction of substituents on the three benzene rings within the terphenyl system disrupts the resonance-stabilized states, hindering the high-conductance electron transport pathway. In addition, our work highlights the importance of noncovalent dimeric interactions in molecular electronics that can be leveraged for the design of materials for bulk measurements. MD simulations are used to understand the stacking conformations for various amino-*p*-terphenyl derivatives, and NEGF-DFT calculations are carried out to understand the electron transport behavior observed in single molecule experiments. Overall, our work highlights the formation of anchor groups in molecular junctions containing only one preinstalled anchor, which enhances the chemical toolbox available for molecular electronics.

■ ASSOCIATED CONTENT

Supporting Information

The Supporting Information is available free of charge at https://pubs.acs.org/doi/10.1021/acs.jpcc.5c06124.

> Additional details for experimental and computational methods, including synthetic procedures, characterization data such as mass spectrometry and NMR analysis for all compounds, additional single-molecule conductance measurements, bulk spectroscopic and electrochemical analyses, molecular dynamics simulations, and quantum mechanical and transmission function calculations in this work (PDF)

■ AUTHOR INFORMATION

Corresponding Author

Charles M. Schroeder − *Department of Chemical and Biomolecular Engineering, University of Illinois at Urbana−Champaign, Urbana, Illinois 61801, United States; Beckman Institute for Advanced Science and Technology, Department of Materials Science and Engineering, Department of Chemistry, Center for Biophysics and Quantitative Biology, Department of Bioengineering, and Materials Research Laboratory, University of Illinois at Urbana−Champaign, Urbana, Illinois 61801, United States;* Present Address: Department of Chemical and Biological Engineering, Princeton University, Princeton, NJ 08544; orcid.org/0000-0001-6023-2274; Email: cschroeder@princeton.edu

Authors

Rajarshi Samajdar − *Department of Chemical and Biomolecular Engineering, University of Illinois at Urbana−Champaign, Urbana, Illinois 61801, United States; Beckman Institute for Advanced Science and Technology, University of Illinois at Urbana−Champaign, Urbana, Illinois 61801, United States*

Hao Yang − *Beckman Institute for Advanced Science and Technology and Department of Materials Science and Engineering, University of Illinois at Urbana−Champaign, Urbana, Illinois 61801, United States*

Seungjoo Yi − *Beckman Institute for Advanced Science and Technology and Department of Materials Science and Engineering, University of Illinois at Urbana−Champaign, Urbana, Illinois 61801, United States*

Chun-I. Wang − *Department of Chemistry, University of Illinois at Urbana−Champaign, Urbana, Illinois 61801, United States*

Seth T. Putnam − *Department of Chemistry, University of Illinois at Urbana−Champaign, Urbana, Illinois 61801, United States;* orcid.org/0000-0003-2912-742X

Michael A. Pence − *Beckman Institute for Advanced Science and Technology and Department of Chemistry, University of Illinois at Urbana−Champaign, Urbana, Illinois 61801, United States;* orcid.org/0000-0001-5880-9812

Gavin S. Lindsay − *Department of Chemistry, University of Illinois at Urbana−Champaign, Urbana, Illinois 61801, United States*

Moeen Meigooni − *Beckman Institute for Advanced Science and Technology and Center for Biophysics and Quantitative Biology, University of Illinois at Urbana−Champaign, Urbana, Illinois 61801, United States*

Xiaolin Liu − *Department of Chemistry, University of Illinois at Urbana−Champaign, Urbana, Illinois 61801, United States;* orcid.org/0000-0002-6909-117X

Jitong Ren − *Department of Chemical and Biomolecular Engineering, University of Illinois at Urbana−Champaign, Urbana, Illinois 61801, United States; Beckman Institute for Advanced Science and Technology, University of Illinois at Urbana−Champaign, Urbana, Illinois 61801, United States*

Jeffrey S. Moore − *Beckman Institute for Advanced Science and Technology, Department of Materials Science and Engineering, and Department of Chemistry, University of Illinois at Urbana−Champaign, Urbana, Illinois 61801, United States;* orcid.org/0000-0001-5841-6269

Emad Tajkhorshid − *Beckman Institute for Advanced Science and Technology, Department of Chemistry, Center for Biophysics and Quantitative Biology, Department of Biochemistry, and Department of Bioengineering, University of Illinois at Urbana−Champaign, Urbana, Illinois 61801, United States;* orcid.org/0000-0001-8434-1010

Andrew A. Gewirth − *Department of Chemistry, University of Illinois at Urbana−Champaign, Urbana, Illinois 61801, United States;* orcid.org/0000-0003-4400-9907

Joaquín Rodríguez-López − *Beckman Institute for Advanced Science and Technology, Department of Chemistry, and Materials Research Laboratory, University of Illinois at Urbana−Champaign, Urbana, Illinois 61801, United States;* orcid.org/0000-0003-4346-4668

Nicholas E. Jackson − *Beckman Institute for Advanced Science and Technology and Department of Chemistry, University of Illinois at Urbana−Champaign, Urbana, Illinois 61801, United States;* orcid.org/0000-0002-1470-1903

Complete contact information is available at:
https://pubs.acs.org/10.1021/acs.jpcc.5c06124

Author Contributions

○R.S., H.Y. and S.Y. contributed equally, co-first author. R.S., H.Y., S.Y., and C.M.S. conceived this study. R.S. and H.Y. performed STM-BJ experiments, data analysis, and machine learning analysis. S.Y. performed chemical synthesis and characterization. C.W. performed MD simulations. M.P. and S.P. carried out bulk electrochemistry and spectroscopy experiments. G.L. and S.P. performed SERS experiments. R.S. performed the NEGF-DFT calculations. M.M., X.L., J.R. assisted in experiments and simulations. The manuscript was written by R.S., H.Y. and C.M.S. with contribution from all authors.

Author Contributions

⊗C.W. and S.T.P. contributed equally, co-second author.

Notes

The authors declare no competing financial interest.

■ ACKNOWLEDGMENTS

This work was supported by the U.S. Department of Energy, Office of Science, Basic Energy Sciences under Award No. DE-SC0022035 for H.Y., X.L., M.M., J.S.M., E.T., and C.M.S., the National Science Foundation under Award 2227399 and the Army Research Office under Cooperative Agreement Number W911NF-22-2-0246 for R.S. and C.M.S. The views and conclusions contained in this document are those of the authors and should not be interpreted as representing the official policies, either expressed or implied, of the Army Research Office or the U.S. Government. The U.S. Government is authorized to reproduce and distribute reprints for Government purposes notwithstanding any copyright notation herein. This work was supported by the Molecule Maker Lab Institute, an AI Research Institutes program supported by the US National Science Foundation under grant no. 2019897 for S.Y. We gratefully acknowledge Furong Sun and the UIUC Mass Spectrometry Lab. S.P. is grateful for support from the National Science Foundation Graduate Research Fellowship. M.P. is grateful for the support of Beckman Institute for Advanced Science and Technology Graduate Fellows Program with support from the Arnold and Mabel Beckman Foundation.

■ REFERENCES

(1) Chen, H.; Fraser Stoddart, J. From molecular to supramolecular electronics. *Nat. Rev. Mater.* **2021**, *6* (9), 804−828.

(2) Li, S.; Yu, H.; Chen, X.; Gewirth, A. A.; Moore, J. S.; Schroeder, C. M. Covalent Ag−C bonding contacts from unprotected terminal acetylenes for molecular junctions. *Nano Lett.* **2020**, *20* (7), 5490−5495.

(3) Hong, W.; Manrique, D. Z.; Moreno-García, P.; Gulcur, M.; Mishchenko, A.; Lambert, C. J.; Bryce, M. R.; Wandlowski, T. Single molecular conductance of tolanes: experimental and theoretical study on the junction evolution dependent on the anchoring group. *J. Am. Chem. Soc.* **2012**, *134* (4), 2292−2304.

(4) Kaliginedi, V.; Rudnev, A. V.; Moreno-García, P.; Baghernejad, M.; Huang, C.; Hong, W.; Wandlowski, T. Promising anchoring groups for single-molecule conductance measurements. *Phys. Chem. Chem. Phys.* **2014**, *16* (43), 23529−23539.

(5) Ward, J. S.; Vezzoli, A.; Wells, C.; Bailey, S.; Jarvis, S. P.; Lambert, C. J.; Robertson, C.; Nichols, R. J.; Higgins, S. J. A Systematic Study of Methyl Carbodithioate Esters as Effective Gold Contact Groups for Single-Molecule Electronics. *Angew. Chem. Int. Ed.* **2024**, *63* (31), No. e202403577.

(6) Magyarkuti, A.; Adak, O.; Halbritter, A.; Venkataraman, L. Electronic and mechanical characteristics of stacked dimer molecular junctions. *Nanoscale* **2018**, *10* (7), 3362−3368.

(7) Quek, S. Y.; Kamenetska, M.; Steigerwald, M. L.; Choi, H. J.; Louie, S. G.; Hybertsen, M. S.; Neaton, J. B.; Venkataraman, L. Mechanically controlled binary conductance switching of a single-molecule junction. *Nat. Nanotechnol.* **2009**, *4* (4), 230−234.

(8) Inkpen, M. S.; Liu, Z. F.; Li, H.; Campos, L. M.; Neaton, J. B.; Venkataraman, L. Non-chemisorbed gold−sulfur binding prevails in self-assembled monolayers. *Nat. Chem.* **2019**, *11* (4), 351−358.

(9) Kamenetska, M.; Quek, S. Y.; Whalley, A. C.; Steigerwald, M. L.; Choi, H. J.; Louie, S. G.; Nuckolls, C.; Hybertsen, M. S.; Neaton, J. B.; Venkataraman, L. Conductance and geometry of pyridine-linked single-molecule junctions. *J. Am. Chem. Soc.* **2010**, *132* (19), 6817−6821.

(10) Yu, H.; Li, S.; Schwieter, K. E.; Liu, Y.; Sun, B.; Moore, J. S.; Schroeder, C. M. Charge transport in sequence-defined conjugated oligomers. *J. Am. Chem. Soc.* **2020**, *142* (10), 4852−4861.

(11) Cheng, Z. L.; Skouta, R.; Vazquez, H.; Widawsky, J. R.; Schneebeli, S.; Chen, W.; Hybertsen, M. S.; Breslow, R.; Venkataraman, L. In situ formation of highly conducting covalent Au−C contacts for single-molecule junctions. *Nat. Nanotechnol.* **2011**, *6* (6), 353−357.

(12) Chen, W.; Widawsky, J. R.; Vázquez, H.; Schneebeli, S. T.; Hybertsen, M. T.; Breslow, R.; Venkataraman, L. Highly conducting π-conjugated molecular junctions covalently bonded to gold electrodes. *J. Am. Chem. Soc.* **2011**, *133* (43), 17160−17163.

(13) Starr, R. L.; Fu, T.; Doud, E. A.; Stone, I.; Roy, X.; Venkataraman, L. Gold−carbon contacts from oxidative addition of aryl iodides. *J. Am. Chem. Soc.* **2020**, *142* (15), 7128−7133.

(14) Bejarano, F.; Olavarria-Contreras, I. J.; Droghetti, A.; Rungger, I.; Rudnev, A.; Gutiérrez, D.; Mas-Torrent, M.; Veciana, J.; van der Zant, H. S. J.; Rovira, C.; Burzurí, E.; Crivillers, N. Robust organic radical molecular junctions using acetylene terminated groups for C−Au bond formation. *J. Am. Chem. Soc.* **2018**, *140* (5), 1691−1696.

(15) Pla-Vilanova, P.; Aragonès, A. C.; Ciampi, S.; Sanz, F.; Darwish, N.; Diez-Perez, I. The spontaneous formation of single-molecule junctions via terminal alkynes. *Nanotechnology* **2015**, *26* (38), 381001.

(16) Peiris, C. R.; Vogel, Y. B.; Le Brun, A. P.; Aragonès, A. C.; Coote, M. L.; Díez-Pérez, I.; Ciampi, S.; Darwish, N. Metal−single-molecule−semiconductor junctions formed by a radical reaction bridging gold and silicon electrodes. *J. Am. Chem. Soc.* **2019**, *141* (37), 14788−14797.

(17) Hines, T.; Díez-Pérez, I.; Nakamura, H.; Shimazaki, T.; Asai, Y.; Tao, N. Controlling formation of single-molecule junctions by electrochemical reduction of diazonium terminal groups. *J. Am. Chem. Soc.* **2013**, *135* (9), 3319−3322.

(18) Huang, X.; Tang, C.; Li, J.; Chen, L.-C.; Zheng, J.; Zhang, P.; Le, J.; Li, R.; Li, X.; Liu, J.; Yang, Y.; Shi, J.; Chen, Z.; Bai, M.; Zhang, H. L.; Xia, H.; Cheng, J.; Tian, Z. Q.; Hong, W. Electric field−induced selective catalysis of single-molecule reaction. *Sci. Adv.* **2019**, *5* (6), No. eaaw3072.

(19) Lin, J.; Lv, Y.; Song, K.; Song, X.; Zang, H.; Du, P.; Zang, Y.; Zhu, D. Cleavage of non-polar C(sp^2)−C(sp^2) bonds in cycloparaphenylenes via electric field-catalyzed electrophilic aromatic substitution. *Nat. Commun.* **2023**, *14* (1), 293.

(20) Aragones, A. C.; Haworth, N. L.; Darwish, N.; Ciampi, S.; Mannix, E. J.; Wallace, G. G.; Diez-Perez, I.; Coote, M. L. Electrostatic catalysis of a Diels−Alder reaction. *Nature* **2016**, *531* (7592), 88−91.

(21) Martín, S.; Grace, I.; Bryce, M. R.; Wang, C.; Jitchati, R.; Batsanov, A. S.; Higgins, S. J.; Lambert, C. J.; Nichols, R. J. Identifying

diversity in nanoscale electrical break junctions. *J. Am. Chem. Soc.* **2010**, *132* (26), 9157−9164.

(22) Frisenda, R.; Janssen, V. A. E. C.; Grozema, F. C.; Van Der Zant, H. S. J.; Renaud, N. Mechanically controlled quantum interference in individual π-stacked dimers. *Nat. Chem.* **2016**, *8* (12), 1099−1104.

(23) Wei, Y.; Li, L.; Greenwald, J. E.; Venkataraman, L. Voltage-modulated van der Waals interaction in single-molecule junctions. *Nano Lett.* **2023**, *23* (2), 567−572.

(24) Yu, H.; Li, J.; Li, S.; Liu, Y.; Jackson, N. E.; Moore, J. S.; Schroeder, C. M. Efficient intermolecular charge transport in π-stacked pyridinium dimers using cucurbit[8]uril supramolecular complexes. *J. Am. Chem. Soc.* **2022**, *144* (7), 3162−3173.

(25) Coropceanu, V.; Cornil, J.; da Silva Filho, D. A.; Olivier, Y.; Silbey, R.; Brédas, J.-L. Charge transport in organic semiconductors. *Chem. Rev.* **2007**, *107* (4), 926−952.

(26) Yi, Y.; Coropceanu, V.; Brédas, J.-L. A comparative theoretical study of exciton-dissociation and charge-recombination processes in oligothiophene/fullerene and oligothiophene/perylenediimide complexes for organic solar cells. *J. Mater. Chem.* **2011**, *21* (5), 1479−1486.

(27) Solomon, G. C.; Herrmann, C.; Vura-Weis, J.; Wasielewski, M. R.; Ratner, M. A. The chameleonic nature of electron transport through π-stacked systems. *J. Am. Chem. Soc.* **2010**, *132* (23), 7887−7889.

(28) Delgado, M. C. R.; Kim, E.-G.; Filho, D. A. d. S.; Bredas, J. L. Tuning the charge-transport parameters of perylene diimide single crystals via end and/or core functionalization: a density functional theory investigation. *J. Am. Chem. Soc.* **2010**, *132* (10), 3375−3387.

(29) Pan, X.; Montes, E.; Rojas, W. Y.; Lawson, B.; Vázquez, H.; Kamenetska, M. Cooperative self-assembly of dimer junctions driven by π stacking leads to conductance enhancement. *Nano Lett.* **2023**, *23* (15), 6937−6943.

(30) Tang, Y.; Zhou, Y.; Zhou, D.; Chen, Y.; Xiao, Z.; Shi, J.; Liu, J.; Hong, W. Electric field-induced assembly in single-stacking terphenyl junctions. *J. Am. Chem. Soc.* **2020**, *142* (45), 19101−19109.

(31) Wang, W.; Angello, N. H.; Blair, D. J.; Tyrikos-Ergas, T.; Krueger, W. H.; Medine, K. N. S.; LaPorte, A. J.; Berger, J. M.; Burke, M. D. Rapid automated iterative small-molecule synthesis. *Nat. Synth.* **2024**, *3* (8), 1031−1038.

(32) Li, S.; Yu, H.; Schwieter, K.; Chen, K.; Li, B.; Liu, Y.; Moore, J. S.; Schroeder, C. M. Charge transport and quantum interference effects in oxazole-terminated conjugated oligomers. *J. Am. Chem. Soc.* **2019**, *141* (4), 16079−16084.

(33) Li, B.; Yu, H.; Montoto, E. C.; Liu, Y.; Li, S.; Schwieter, K.; Rodríguez-López, J.; Moore, J. S.; Schroeder, C. M. Intrachain charge transport through conjugated donor−acceptor oligomers. *ACS Appl. Electron. Mater.* **2019**, *1* (1), 7−12.

(34) Ciampi, S.; Darwish, N.; Aitken, H. M.; Díez-Pérez, I.; Coote, M. L. Harnessing electrostatic catalysis in single molecule, electrochemical and chemical systems: a rapidly growing experimental tool box. *Chem. Soc. Rev.* **2018**, *47* (14), 5146−5164.

(35) Angello, N. H.; Friday, D. M.; Hwang, C.; Yi, S.; Cheng, A. H.; Torres-Flores, T. C.; Jira, E. R.; Wang, W.; Aspuru-Guzik, A.; Burke, M. D.; Schroeder, C. M.; Diao, Y.; Jackson, N. E. Closed-loop transfer enables artificial intelligence to yield chemical knowledge. *Nature* **2024**, *633* (8029), 351−358.

(36) Venkataraman, L.; Klare, J. E.; Tam, I. W.; Nuckolls, C.; Hybertsen, M. S.; Steigerwald, M. L. Single-molecule circuits with well-defined molecular conductance. *Nano Lett.* **2006**, *6* (3), 458−462.

(37) Makk, P.; Tomaszewski, D.; Martinek, J.; Balogh, Z.; Csonka, S.; Wawrzyniak, M.; Frei, M.; Venkataraman, L.; Halbritter, A. Correlation analysis of atomic and single-molecule junction conductance. *ACS Nano* **2012**, *6* (4), 3411−3423.

(38) Stefani, D.; Guo, C.; Ornago, L.; Cabosart, D.; El Abbassi, M.; Sheves, M.; Cahen, D.; Van Der Zant, H. S. J. Conformation-dependent charge transport through short peptides. *Nanoscale* **2021**, *13* (5), 3002−3009.

(39) Lin, L.; Tang, C.; Dong, G.; Chen, Z.; Pan, Z.; Liu, J.; Yang, Y.; Shi, J.; Ji, R.; Hong, W. Spectral clustering to analyze the hidden events in single-molecule break junctions. *J. Phys. Chem. C* **2021**, *125* (6), 3623−3630.

(40) Li, J.; Pudar, S.; Yu, H.; Li, S.; Moore, J. S.; Rodríguez-López, J.; Jackson, N. E.; Schroeder, C. M. Reversible switching of molecular conductance in viologens is controlled by the electrochemical environment. *J. Phys. Chem. C* **2021**, *125* (40), 21862−21872.

(41) Hosseini, S.; Thapa, B.; Medeiros, M. J.; Pasciak, E. M.; Pence, M. A.; Twum, E. B.; Karty, J. A.; Gao, X.; Raghavachari, K.; Peters, D. G.; Mubarak, M. S. Electrosynthesis of a biaurone by controlled dimerization of flavone: mechanistic insight and large-scale application. *J. Org. Chem.* **2020**, *85* (16), 10658−10669.

(42) Lindsay, G. S.; Rohde, D.; Bernhard, T.; Zarwell, S.; Schmidt, R.; Bandas, C. D.; Gewirth, A. A. Effect of Ni on electroless Cu plating rates in the presence of 2,2′-bipyridyl and 2-mercaptobenzothiazole. *J. Electrochem. Soc.* **2023**, *170* (10), 102502.

(43) Kumar, S.; Rosenberg, J. M.; Bouzida, D.; Swendsen, R. H.; Kollman, P. A. The weighted histogram analysis method for free-energy calculations on biomolecules. I. The method. *J. Comput. Chem.* **1992**, *13* (8), 1011−1021.

(44) Jorgensen, W. L.; Tirado-Rives, J. Potential energy functions for atomic-level simulations of water and organic and biomolecular systems. *Proc. Natl. Acad. Sci. U.S.A.* **2005**, *102* (19), 6665−6670.

(45) Dodda, L. S.; Vilseck, J. Z.; Tirado-Rives, J.; Jorgensen, W. L. 1.14 CM1A-LBCC: localized bond-charge corrected CM1A charges for condensed-phase simulations. *J. Phys. Chem. B* **2017**, *121* (15), 3864−3870.

(46) Dodda, L. S.; Cabeza de Vaca, I.; Tirado-Rives, J.; Jorgensen, W. L. LigParGen web server: an automatic OPLS-AA parameter generator for organic ligands. *Nucleic Acids Res.* **2017**, *45* (W1), W331−W336.

(47) Martínez, L.; Andrade, R.; Birgin, E. G.; Martínez, J. M. PACKMOL: A package for building initial configurations for molecular dynamics simulations. *J. Comput. Chem.* **2009**, *30* (13), 2157−2164.

(48) Thompson, A. P.; Aktulga, H. M.; Berger, R.; Bolintineanu, D. S.; Brown, W. M.; Crozier, P. S.; in 't Veld, P. J.; Kohlmeyer, A.; Moore, S. G.; Nguyen, T. D.; Shan, R.; Stevens, M. J.; Tranchida, J.; Trott, C.; Plimpton, S. J. LAMMPS—a flexible simulation tool for particle-based materials modeling at the atomic, meso, and continuum scales. *Comput. Phys. Commun.* **2022**, *271*, 108171.

(49) Brandbyge, M.; Mozos, J.-L.; Ordejón, P.; Taylor, J.; Stokbro, K. Density-functional method for nonequilibrium electron transport. *Phys. Rev. B* **2002**, *65* (16), 165401.

(50) Soler, J. M.; Artacho, E.; Gale, J. D.; García, A.; Junquera, J.; Ordejón, P.; Sánchez-Portal, D. The SIESTA method for ab initio order-N materials simulation. *J. Phys.: Condens. Matter* **2002**, *14* (11), 2745.

(51) Papior, N.; Lorente, N.; Frederiksen, T.; García, A.; Brandbyge, M. Improvements on non-equilibrium and transport Green function techniques: The next-generation TranSIESTA. *Comput. Phys. Commun.* **2017**, *212*, 8−24.

(52) Perdew, J. P.; Burke, K.; Ernzerhof, M. Generalized gradient approximation made simple. *Phys. Rev. Lett.* **1996**, *77* (18), 3865.

(53) Li, S.; Jira, E. R.; Angello, N. H.; Li, J.; Yu, H.; Moore, J. S.; Diao, Y.; Burke, M. D.; Schroeder, C. M. Using automated synthesis to understand the role of side chains on molecular charge transport. *Nat. Commun.* **2022**, *13* (1), 2102.

(54) Gillis, E. P.; Burke, M. D. A simple and modular strategy for small molecule synthesis: iterative Suzuki−Miyaura coupling of B-protected haloboronic acid building blocks. *J. Am. Chem. Soc.* **2007**, *129* (21), 6716−6717.

(55) Ryan, S. T. J.; Young, R. M.; Henkelis, J. J.; Hafezi, N.; Vermeulen, N. A.; Hennig, A.; Dale, E. J.; Wu, Y.; Krzyaniak, M. D.; Fox, A.; et al. Energy and electron transfer dynamics within a series of perylene diimide/cyclophane systems. *J. Am. Chem. Soc.* **2015**, *137* (48), 15299−15307.

(56) Wakamatsu, S.; Akiba, U.; Fujihira, M. Electronic tunneling through a single molecule embedded in self-assembled monolayer matrices. *Colloids Surf., A* **2002**, *198*, 785−790.

(57) Duan, L.; Garrett, S. J. An investigation of rigid p-methylterphenyl thiol self-assembled monolayers on Au (111) using reflection−absorption infrared spectroscopy and scanning tunneling microscopy. *J. Phys. Chem. B* **2001**, *105*, 9812−9816.

(58) Heimel, G.; Somitsch, D.; Knoll, P.; Zojer, E. Ab initio study of vibrational anharmonic coupling effects in oligo (para-phenylenes). *J. Chem. Phys.* **2002**, *116*, 10921−10931.

(59) Maya, F.; Tour, J. M. Synthesis of terphenyl oligomers as molecular electronic device candidates. *Tetrahedron* **2004**, *60*, 81−92.

(60) Feng, A.; Zhou, Y.; Al-Shebami, M. A. Y.; Chen, L.; Pan, Z.; Xu, W.; Zhao, S.; Zeng, B.; Xiao, Z.; Yang, Y.; Hong, W. σ−σ Stacked supramolecular junctions. *Nat. Chem.* **2022**, *14* (10), 1158−1164.

(61) Samajdar, R.; Meigooni, M.; Yang, H.; Li, J.; Liu, X.; Jackson, N. E.; Mosquera, M. A.; Tajkhorshid, E.; Schroeder, C. M. Secondary structure determines electron transport in peptides. *Proc. Natl. Acad. Sci. U.S.A.* **2024**, *121*, No. e2403324121.

(62) Liu, X.; Yang, H.; Harb, H.; Samajdar, R.; Woods, T. J.; Lin, O.; Chen, Q.; Romo, A. I. B.; Rodríguez-López, J.; Assary, R. S.; Moore, J. S.; Schroeder, C. M. Shape-persistent ladder molecules exhibit nanogap-independent conductance in single-molecule junctions. *Nat. Chem.* **2024**, *16*, 1772−1780.

(63) Adak, O.; Rosenthal, E.; Meisner, J.; Andrade, E. F.; Pasupathy, A. N.; Nuckolls, C.; Hybertsen, M. S.; Venkataraman, L. Flicker noise as a probe of electronic interaction at metal−single molecule interfaces. *Nano Lett.* **2015**, *15* (6), 4143−4149.

(64) Fu, T.; Smith, S.; Camarasa-Gómez, M.; Yu, X.; Xue, J.; Nuckolls, C.; Evers, F.; Venkataraman, L.; Wei, S. Enhanced coupling through π-stacking in imidazole-based molecular junctions. *Chem. Sci.* **2019**, *10* (43), 9998−10002.

(65) Tan, Y.; Li, J.; Li, S.; Yang, H.; Chi, T.; Shiring, S. B.; Liu, K.; Savoie, B. M.; Boudouris, B. W.; Schroeder, C. M. Enhanced electron transport in nonconjugated radical oligomers occurs by tunneling. *Nano Lett.* **2023**, *23* (13), 5951−5958.

(66) Bard, A. J.; Faulkner, L. R. *Electrochemical Methods: Fundamentals and Applications*; Wiley: New York, 2001; pp 1364−1365.

(67) Dunsch, L.; Rapta, P.; Schulte, N.; Schlüter, A. D. Structural Dependence of Redox-Induced Dimerization as Studied by In Situ ESR/UV/Vis-NIR Spectroelectrochemistry: The Fluoranthenopyracylene Oligomers. *Angew. Chem., Int. Ed.* **2002**, *41* (12), 2082−2086.

(68) Shao, C.; Grüne, M.; Stolte, M.; Würthner, F. Perylene Bisimide Dimer Aggregates: Fundamental Insights into Self-Assembly by NMR and UV/Vis Spectroscopy. *Chem. - Eur. J.* **2012**, *18* (43), 13665−13677.

(69) Ahmad, R.; Boubekeur-Lecaque, L.; Nguyen, M.; Lau-Truong, S.; Lamouri, A.; Decorse, P.; Galtayries, A.; Pinson, J.; Felidj, N.; Mangeney, C. Tailoring the Surface Chemistry of Gold Nanorods through Au−C/Ag−C Covalent Bonds Using Aryl Diazonium Salts. *J. Phys. Chem. C* **2014**, *118* (33), 19098−19105.

(70) Guo, L.; Ma, L.; Zhang, Y.; Cheng, X.; Xu, Y.; Wang, J.; Wang, E.; Peng, Z. Spectroscopic Identification of the Au−C Bond Formation upon Electroreduction of an Aryl Diazonium Salt on Gold. *Langmuir* **2016**, *32* (44), 11514−11519.

(71) Stone, I.; Starr, R. L.; Zang, Y.; Nuckolls, C.; Steigerwald, M. L.; Lambert, T. H.; Roy, X.; Venkataraman, L. A Single-Molecule Blueprint for Synthesis. *Nat. Rev. Chem.* **2021**, *5* (10), 695−710.